

# Catalysis Science & Technology

Accepted Manuscript

This article can be cited before page numbers have been issued, to do this please use: H. Wen, J. Xie, Y. Zhou, Y. Zhou and J. Wang, *Catal. Sci. Technol.*, 2019, DOI: 10.1039/C9CY01329F.



This is an Accepted Manuscript, which has been through the Royal Society of Chemistry peer review process and has been accepted for publication.

Accepted Manuscripts are published online shortly after acceptance, before technical editing, formatting and proof reading. Using this free service, authors can make their results available to the community, in citable form, before we publish the edited article. We will replace this Accepted Manuscript with the edited and formatted Advance Article as soon as it is available.

You can find more information about Accepted Manuscripts in the [Information for Authors](#).

Please note that technical editing may introduce minor changes to the text and/or graphics, which may alter content. The journal's standard [Terms & Conditions](#) and the [Ethical guidelines](#) still apply. In no event shall the Royal Society of Chemistry be held responsible for any errors or omissions in this Accepted Manuscript or any consequences arising from the use of any information it contains.

## ARTICLE

# Straightforward synthesis of MTW-type magnesium silicalite for CO<sub>2</sub> fixation with epoxides under mild conditions†

Haimeng Wen,<sup>a</sup> Jingyan Xie,<sup>a,b</sup> Yang Zhou,<sup>a</sup> Yu Zhou\*<sup>a</sup> and Jun Wang\*<sup>a</sup>Received 00th January 20xx,  
Accepted 00th January 20xx

DOI: 10.1039/x0xx00000x

Aluminum-free magnesium silicalite with MTW topology (Mg-Si-ZSM-12) was fabricated in a straightforward hydrothermal synthesis route involving an initial acid co-hydrolysis step. Mg incorporation endowed superior basic properties in the MTW framework, as illustrated by CO<sub>2</sub> sorption and temperature programmed desorption plus the activity in a typical basic reaction, Knoevenagel condensation. Mg-Si-ZSM-12 catalyzed coupling of atmospheric CO<sub>2</sub> with epoxides led the efficient production of cyclic carbonates with high yield and selectivity at relatively low temperature (down to 60 °C). The present strategy afforded a kind of zeolitic solid base with regular 12-membered ring microporous channels that possesses potential application in CO<sub>2</sub> fixation.

## Introduction

Carbon dioxide (CO<sub>2</sub>) conversion into value-added chemicals have attracted significant growing academic and industrial attentions.<sup>1-3</sup> The importance of this issue is not only because CO<sub>2</sub> is one of the main contributors to the greenhouse effect for climate change, but also CO<sub>2</sub> is widely regarded as a naturally abundant, inexpensive, eco-friendly and renewable C1 resource.<sup>4-6</sup> So far, various chemicals have been produced through CO<sub>2</sub> transformation,<sup>7-10</sup> and cycloaddition of CO<sub>2</sub> with epoxides is a promising methodology to produce cyclic carbonates that have found wide applications in the pharmaceutical and fine chemical industries.<sup>11-13</sup> Great efforts have been denoted to design efficient catalysts such as metal complexes, organic molecules, metal organic frameworks (MOFs), covalent organic frameworks (COFs) and porous organic polymers (POPs).<sup>14-18</sup> Despite these progresses, it is exceedingly desirable but still one challenge to develop easily available heterogeneous catalysts to catalyze the CO<sub>2</sub> fixation under mild conditions.

Porous materials are preferred in a heterogeneous catalysis due to the abundant porosity that can improve the dispersion and accessibility of active sites. Zeolites, crystalline aluminosilicates, are among the most important porous materials and have been extensively applied as adsorbents and catalysts in industry, attributable to their large surface areas, regular microporous channels, high thermal/hydrothermal stability, adjustable chemical composition, topology and morphology.<sup>19-21</sup> Up to now, only several zeolites and their analogues have been tried in the CO<sub>2</sub> cycloaddition with epoxides and the reaction was normally carried out under harsh

conditions (high temperature and pressure).<sup>22-24</sup> For example, KX and Cs-loaded KX zeolites exhibited low yields in the conversion of high-pressure CO<sub>2</sub> (3.8 MPa) and epoxides at high temperature of 150 °C. The activity was related to the basicity of these zeolites and the one having occluded alkali metal oxides was more active.<sup>22</sup> An organic-inorganic hybrid zeolite with organic structure-directing agents in the MFI-type lamellar structure was active in the coupling of CO<sub>2</sub> (2 MPa) with a variety of epoxides at 140 °C.<sup>23</sup> The zeolite analogues, lanthanide zeolite assembled by [Ln<sub>60</sub>] nanocages with strong basicity, effectively catalyzed the coupling of CO<sub>2</sub> with multiple epoxides in the presence of tetrabutylammonium bromide (TBAB).<sup>24</sup> Therefore, efficient zeolites for the CO<sub>2</sub> conversion via cycloaddition reaction are still to be explored.

Ring-opening *via* nucleophilic attack, CO<sub>2</sub> insertion, and ring-closure with the leaving of nucleophile are the three primary steps in the CO<sub>2</sub> cycloaddition with high energy three-membered heterocyclic compounds such as epoxides.<sup>10-15</sup> Because CO<sub>2</sub> molecules are naturally acidic and inert, strengthening the basicity of a heterogeneous catalyst benefits to promote the CO<sub>2</sub> activation for improving the activity. Such phenomenon was also found in the above-mentioned zeolites catalyzed CO<sub>2</sub> cycloaddition reaction.<sup>22</sup> However, zeolites usually have weak basicity that is disadvantageous for the CO<sub>2</sub> activation in the cycloadditions. The reason is attributable to that the classic zeolites are crystalline aluminosilicates composed of SiO<sub>4</sub> and AlO<sub>4</sub><sup>-</sup> units, and conventional modifications usually generate acid or acid-base sites due to the intrinsic acidity provided by the aluminum (Al) species.<sup>25-28</sup> Several approaches have been proposed to prepare Al-free zeolites to construct basic zeolites and exclude the potential Al species derived shielding on basic sites.<sup>29-31</sup> Compared with post-modifications, straightforward synthesis simplifies the procedure and preserves the zeolitic crystalline microporous channels to a great extent,<sup>32-34</sup> but fabrication of Al-free basic zeolites was extremely scarce in the hydrothermal synthesis. Incorporation of metal ions with low electronegativity can improve the basicity of zeolites.<sup>35-38</sup> Mg-containing Silicalite-1 with MFI topology (MgS-1) was synthesized as efficient zeolitic solid base,<sup>39</sup>

<sup>a</sup> State Key Laboratory of Materials-Oriented Chemical Engineering, College of Chemical Engineering, Nanjing Tech University, Nanjing 210009, Jiangsu, P. R. China. E-mails: njtzhouyu@njtech.edu.cn (Y. Zhou), junwang@njtech.edu.cn (J. Wang)

<sup>b</sup> Maoming Branch R&D Institute, SINOPEC, Maoming 525011, P. R. China.

† These two authors contributed equally: Haimeng Wen and Jingyan Xie. Electronic Supplementary Information (ESI) available: [Figure S1-S9]. See DOI: 10.1039/x0xx00000x

but such methodology has not been expanded to other topological zeolites, due to the synthetic difficulty in the synthesis of metal containing and Al-free zeolites.

In this work, we report the direct synthesis of Al-free MTW-type magnesium silicalite (Mg-Si-ZSM-12) that affords a new kind of zeolitic solid base with large 12-membered ring (12-MR) microporous channels. The synthesis was achieved in a hydrothermal route with an initial acid co-hydrolysis stage that facilitates a fine control of co-hydrolysis and condensation of metal and silica precursors to enable the incorporation of Mg species in the zeolitic skeleton.<sup>40-42</sup> Multiple synthetic parameters were investigated to provide high crystalline zeolite structure. The basicity of Mg-Si-ZSM-12 was illustrated by CO<sub>2</sub> sorption and temperature programmed desorption (CO<sub>2</sub>-TPD) plus the efficiency in a typical basic reaction, Knoevenagel condensation. The topology of zeolites is intrinsically essential for their applications, and herein, we demonstrated that the large 12-MR of Mg-Si-ZSM-12 apparently accelerated the reaction rate and gave high yields in the condensation between various aromatic aldehydes and ethyl cyanoacetate or malononitrile. Owing to the superior basicity, Mg-Si-ZSM-12 was active in the cycloaddition of CO<sub>2</sub> with epoxides under mild conditions. A series of epoxides including the long alkyl chain terminal ones were effectively converted into the corresponding cyclic carbonates by coupling with atmospheric CO<sub>2</sub>. After reaction, the catalyst was readily recovered and reused. The activity of Mg-Si-ZSM-12 was also compared with previous Mg-containing silicalite MgS-1 and commercial solid base MgO.

## Experimental

### Synthesis

MTW-type magnesium silicalite (Mg-Si-ZSM-12), was hydrothermally synthesized in an acidic co-hydrolysis route. Typically, concentrated aqueous hydrochloric acid (HCl, 36.5 wt.%) was slowly dropped into a mixed aqueous solution of TEOS (28.4 wt. % SiO<sub>2</sub>, Shanghai Chem. Reagent Co., AR) and Mg(NO<sub>3</sub>)<sub>2</sub>•6H<sub>2</sub>O (99 wt.%, Sinopharm Chem. Reagent Co., AR) to reach pH=0.8 and then the mixture was stirred at 90 °C for 4 h. The H<sub>2</sub>O/SiO<sub>2</sub> molar ratio was adjusted by evaporation at 100 °C. A slight lower temperature of 90 °C than the boiling point of water (100 °C) was adopted in the initial acid co-hydrolysis step to enable sufficient hydrolysis and condensation of silica precursor tetraethyl orthosilicate (TEOS) and avoid the rapid evaporation of water in the initial stage. After that, the temperature of 100 °C was used to reach more sufficient hydrolysis and condensation of silica precursor.<sup>40,43</sup> Subsequently, tetraethylammonium hydroxide (TEAOH, 25 wt. %, Jintan Huadong Chem. Res. Institute, AR) was dropwise added into the gel, followed by a further aging at room temperature for 24 h. The molar composition of the resulting gel mixture was 40 SiO<sub>2</sub>: 8 TEAOH: 0.8 MgO: 320 H<sub>2</sub>O. The pH value of the gel was then adjusted to be 12.3 by adding alkali source such as sodium hydroxide (NaOH) or potassium hydroxide (KOH). After that, the gel was transferred to a Teflon-lined stainless-steel autoclave and statically crystallized at 140 °C for 14 d. The solid was isolated by centrifugation, washed with water and dried at 100 °C. The obtained as-synthesized sample was calcined at 550 °C for 5 h in air to give the as-calcined product. For

comparison, Mg<sup>2+</sup>-incorporated silicalite-1 sample (MgS-1) was synthesized according to the literature.<sup>39</sup> DOI: 10.1039/C9CY01329F

### Characterization

The crystalline structure was characterized by X-ray diffraction analysis (XRD) with a SmartLab diffractometer from Rigaku equipped with a 9 kW rotating anode Cu source at 45 kV and 100 mA, from 5° to 50° with a scan rate of 0.2° s<sup>-1</sup>. Field-emission scanning electron microscope (SEM) instrument (HITACHI S-4800) was used to reveal the morphology information. Nitrogen sorption experiment for the measurement of surface area and pore volume was carried out at 77 K on a BELSORP-MAX analyzer. The samples were pre-degassed at 300 °C for 3 h. Fourier Transform infrared spectroscopy (FT-IR) spectra were recorded on an Agilent Cary 660 FT-IR instrument in the region 4000-400 cm<sup>-1</sup>. In situ FT-IR spectra were recorded on the Agilent Cary 660 spectrometer equipped with a mercury cadmium telluride (MCT) detector and a Harrick Scientific DRIFTS cell at a resolution of 4 cm<sup>-1</sup>. The samples were pretreated at 473 K for 5 h under N<sub>2</sub> atmosphere. Spectra were collected at 0, 1, 5, 15 and 30 min after adsorption of dynamic CO<sub>2</sub> or epoxypropane stream. Epoxypropane was introduced through bubbling by carrier gas (N<sub>2</sub>). Solid UV-vis spectra were measured on a SHIMADZU UV-2600 spectrometer and barium sulfate (BaSO<sub>4</sub>) was used as an internal standard. Chemical compositions were analyzed by using Jarrell-Ash 1100 inductively coupling plasma (ICP) spectrometer. Temperature programmed desorption of carbon dioxide (CO<sub>2</sub>-TPD) was performed on an instrument of Catalyst Analyzer BELCAT-B. Samples were pretreated at 550 °C for 2 h, and then cooled to 50 °C under helium (He) gas. Adsorption of CO<sub>2</sub> was carried out at 50 °C for 30 min under the flow rate of 30 mL min<sup>-1</sup>. After the samples were purged under He gas for 30 min, the temperature was heated to 700 °C (8 °C min<sup>-1</sup>). The desorbed gas was determined by a Gow-Mac thermal conductivity detector (TCD). Basic sites are determined by using ChemMaster software. <sup>29</sup>Si magic angle spinning nuclear magnetic resonance (MAS NMR) spectrum was obtained on a Bruker Avance III spectrometer at an external magnetic field of 9.4 T with a 7 mm double-tuned MAS probe at a spinning rate of 6 kHz. CO<sub>2</sub> sorption isotherms at 273 and 298 K up to 1.0 bar were recorded on BELSORP-MAX analyser. Isotheric heat of CO<sub>2</sub> adsorption (Q<sub>st</sub>) was calculated according to Clausius-Clapeyron equation by fitting CO<sub>2</sub> isotherms with Virial equation.<sup>44</sup>

### Catalysis test

Knoevenagel condensation of aromatic aldehyde with malononitrile or ethyl cyanoacetate was carried out in a round bottom flask. In a typical run, aromatic aldehyde (8 mmol) and malononitrile or ethyl cyanoacetate (8 mmol) was dissolved in ethanol, followed by addition of catalyst (0.1 g). The reaction mixture was stirred at 70 °C for 4 h. After reaction, the mixture solution was cooled down to room temperature and diluted by ethanol. N-dodecane (0.5 g) as internal standard was added and the reaction mixture was centrifuged to remove the solid catalyst. The products were analyzed by gas chromatograph (GC, Agilent 7890B) equipped with an FID detector and a capillary column (HP-5, 30 m×0.25 mm×0.25 mm).

The synthesis of cyclic carbonates through the cycloaddition of CO<sub>2</sub> with epoxides was performed under atmospheric condition. In a typical procedure, epichlorohydrin (5 mmol), catalyst (0.12 g) and tetrabutylammonium bromide (TBAB, 0.048 g, 3 mol% with respect



Scheme 1 Schematic illustration of the synthesis procedure and structural skeleton of Mg-Si-ZSM-12.

to the substrate) were placed in a 25 mL Schlenk flask with a CO<sub>2</sub> balloon (1.0 bar). The reaction proceeded at the specified temperature for preset time. After reaction, the reaction mixture was diluted with ethyl acetate, followed with the addition of the internal standard *n*-dodecane (0.5 g). The solid catalyst was removed by centrifugation, and the filtrate was analyzed by GC and GC-MS (Bruker Scion 436 GCMS). Reusability was investigated in a five-run recycling test. After reaction, the recovered catalyst was washed with ethanol and charged into next run.

#### Adsorption of bulky epoxide

The adsorption of 1,2-epoxytetradecane was measured in a glass tube. Typically, catalyst (50 mg), 1,2-epoxytetradecane (5 mg) and ethyl acetate (1 mL) were stirred at room temperature for a quarantine period. After that, the solid was removed by filtration and the filtrate was analyzed by GC. The adsorption amounts were determined from the variation in adsorbate concentration.

## Results and discussion

### Formation of magnesium silicalite

Scheme 1 shows the synthetic procedure of MTW-type magnesium silicalite (Mg-Si-ZSM-12) involving an acid co-hydrolysis step. Three typical Mg-Si-ZSM-12 samples were synthesized with the initial gel composition of 40 SiO<sub>2</sub>: 8 TEAOH: 0.4 (0.8 and 1.6) MgO: 320 H<sub>2</sub>O. They are termed Mg-Si-ZSM-12(*n*), in which *n* (*n*=100, 50 and 25) denotes the Si/Mg molar ratio in the gel. XRD patterns of them showed typical diffraction peaks at 2θ values of 7.4°, 8.8°, 20.8° and 23.1° for MTW zeolites (Fig. 1A).<sup>45</sup> No impurity for other phase was observable, revealing the well crystalline structure. The Mg content in the gel affects the synthesis as well as the crystallinity of the product and the highest crystallinity was obtained at *n*=50. Excessive Mg salt in the gel (e.g. *n*=20) caused amorphous structure (Fig. S1†). Because of longer bond length of Mg-O (0.185 nm) in comparison with Si-O (0.161 nm) and Al-O (0.175 nm), incorporation of Mg will distort the tetrahedron inevitably and become a disadvantage for the crystallization.<sup>39,46</sup> Meanwhile, not all of the Mg ions added in the initial stage were incorporated into zeolites, and the dissociative or extra-framework metal ions affect the crystallization.<sup>47,48</sup> The preparation of pure silica ZSM-12 failed in this system, resulting either amorphous structure or no solid after crystallization. This

phenomenon suggests that the presence of Mg<sup>2+</sup> is important for the formation of MTW structure.

DOI: 10.1039/C9CY01329F

Various parameters including the alkali source, gel composition and crystallization condition were investigated to gain insight into the synthesis. Alkali metal ions were vital for the synthesis of zeolites by influencing the crystallization rate, crystal size and morphology.<sup>25,26</sup> Herein, the influence of Na<sup>+</sup> and K<sup>+</sup> cations on the synthesis process was studied by varying the alkali source. In the case of NaOH, Mg-Si-ZSM-12 was synthesized with the crystallization pH value from 11.7 to 12.5, reaching the highest crystallinity at pH=12.3 (Fig. S2A†). By contrast, Mg-Si-ZSM-12 was obtained only with the crystallization at pH=12.5 by using KOH (Fig. S2B†). Further, the synthesis of Mg-Si-ZSM-12 was tried in the co-existence of NaOH and KOH. The suitable pH value during the crystallization was 11.5–11.9 by using equal weight amount NaOH and KOH (Fig. S2C†). These results indicate that both NaOH and KOH are effective in the synthesis, with broader synthesizable scope by using NaOH.

Notably, the water content in the gel is a critical factor. Fig. S2D† shows the XRD patterns of Mg-Si-ZSM-12 samples synthesized with different molar ratios of water to silica in the gel (H<sub>2</sub>O/SiO<sub>2</sub> ratio). Amorphous structure was formed with low H<sub>2</sub>O/SiO<sub>2</sub> ratio (<7), which is assigned to the failure of the dissolution of the raw materials under such conditions. By increasing H<sub>2</sub>O/SiO<sub>2</sub> ratio to 7, only certain feeble characteristic peaks assignable to MTW topology appeared, implying

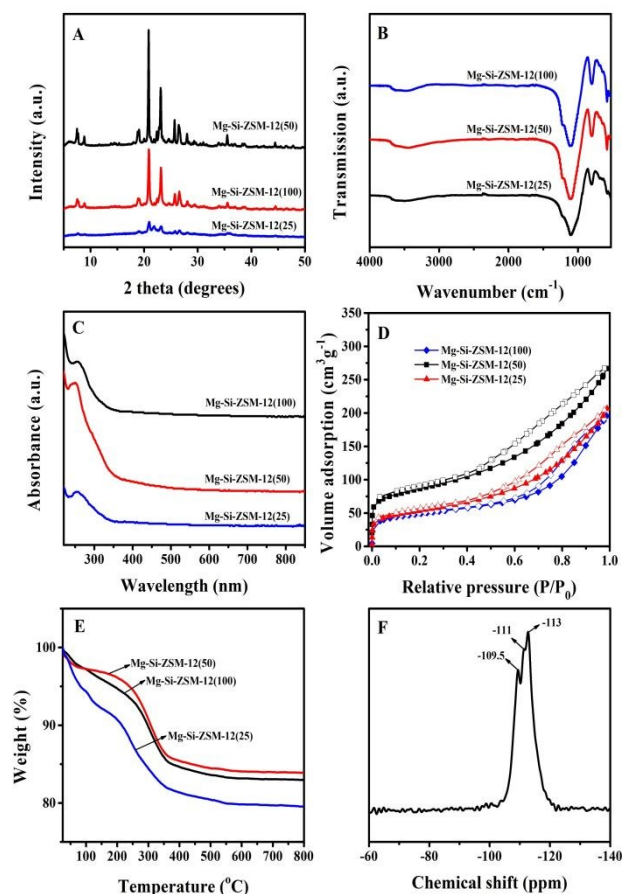


Figure 1 (A) XRD patterns, (B) FT-IR spectra, (C) UV-vis spectra, (D) N<sub>2</sub> sorption isotherms and (E) TG curves of Mg-Si-ZSM-12(*n*) series; (F) <sup>29</sup>Si MAS NMR spectrum of Mg-Si-ZSM-12(50).

Table 1 Textural properties.

Sample	Mg/Si <sup>a</sup> (mol/mol)	Surface area (m <sup>2</sup> g <sup>-1</sup> )	Pore volume (cm <sup>3</sup> g <sup>-1</sup> )	Basic sites (mmol g <sup>-1</sup> )	Unit cell parameters <sup>b</sup>			
					a (nm)	b (nm)	c (nm)	V (nm <sup>3</sup> )
Mg-Si-ZSM-12(100)	0.0079	244	0.32	0.914	24.84	5.03	12.17	1462.30
Mg-Si-ZSM-12(50)	0.0091	312	0.41	1.451	24.93	5.05	12.21	1498.47
Mg-Si-ZSM-12(25)	0.0083	256	0.35	0.892	24.90	5.04	12.19	1479.24

<sup>a</sup>Mg/Si molar ratios in the final solid products. <sup>b</sup>Unit cell parameters determined by using MDI Jade software (Jade 7 XRD Pattern processing Software).

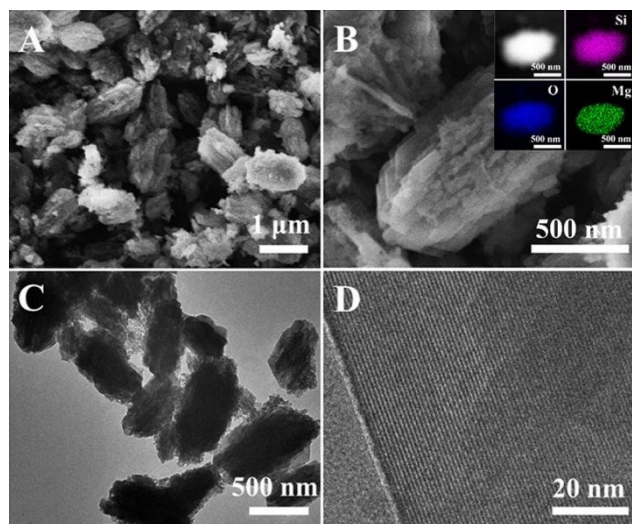


Figure 2 (A, B) SEM images (the inset images are the corresponding energy-dispersive X-ray spectrometry elemental mapping analysis) and (C, D) TEM images of Mg-Si-ZSM-12(50).

the low crystallinity. Well-defined crystal structure emerged as H<sub>2</sub>O/SiO<sub>2</sub> ratio increased to 8. Further increased H<sub>2</sub>O/SiO<sub>2</sub> ratio caused amorphous structure. The crystallization time and template content in the gel were also investigated, giving the highest crystallinity with TEOH/SiO<sub>2</sub> molar ratio of 0.2 (Fig. S3A<sup>†</sup>) and the crystallization time of 14 d (Fig. S3B<sup>†</sup>).

#### Further structural characterization

Systematical structure characterizations were performed on Mg-Si-ZSM-12(*n*) (*n*=100, 50 and 25) zeolites. Their chemical composition was analysed by ICP and the results in Table 1 indicate the incorporation of Mg ions. The molar ratio of Mg to Si ( $n_{\text{Mg}}/n_{\text{Si}}$ ) was 0.0079 for *n*=100. This value varies to 0.0091 and 0.0083 for *n*=50 and 25. Lower  $n_{\text{Mg}}/n_{\text{Si}}$  values were in the final products than those in the gel, due to that part Mg species stay in the solution after crystallization. Mg-Si-ZSM-12(25) has lower Mg content than Mg-Si-ZSM-12(50), attributable to the salt effect that is frequently observed in the synthesis of zeolite, especially for heteroatomic zeolite.<sup>40,49,50</sup> The crystallization would be disturbed when higher condensation of metal salt existed in the synthetic system, and thus cause declined content of heteroatom in the solid. The unit cell parameters are calculated from XRD patterns and summarized in Table 1. The unit cell of Mg-Si-ZSM-12(*n*) expands with Mg loadings and achieves the maximum at *n*=50 (Table 1), suggesting the Mg incorporation.

In the FT-IR spectra (Fig. 1B), the band near 580 cm<sup>-1</sup> is

characteristic of stretching vibrations of the double five-membered rings of the MTW structure.<sup>51</sup> Fig. 1C shows the UV-vis spectra. No absorption in the 220-800 nm range is observed over the Mg-free sample,<sup>52</sup> while all the Mg-Si-ZSM-12(*n*) samples exhibited a distinct absorption band at 260 nm, same as the Mg<sup>2+</sup>-incorporated silicalite-1.<sup>39</sup> Such a signal can be assigned to the excitation of O atoms around the framework Mg species, which is highly distorted or possesses vacancies compared to the regular MgO topology.<sup>53</sup>

The porosity was quantitatively measured by N<sub>2</sub> sorption experiment. The corresponding N<sub>2</sub> sorption isotherms are presented in Fig. 1D and the related textural properties are shown in Table 1. All the samples have the isotherms of mixed type I and IV, according to the IUPAC classification. A H3 type hysteresis loop is observed at region of P/P<sub>0</sub>>0.4 due to capillary condensation, implying the formation of mesopores derived from the aggregation of small particles. These features demonstrate the co-existence of micropores and mesopores.<sup>54</sup> The presence of abundant mesopores was further reflected by the relative narrow pore size distribution with the most probable pore size located at 3.7 nm (Fig. S4<sup>†</sup>). All the samples possess high surface area and large pore volume, similar to previously reported ZSM-12.<sup>55</sup> The concrete values depend on the Mg content. Mg-Si-ZSM-12(50) has the highest surface area of 312

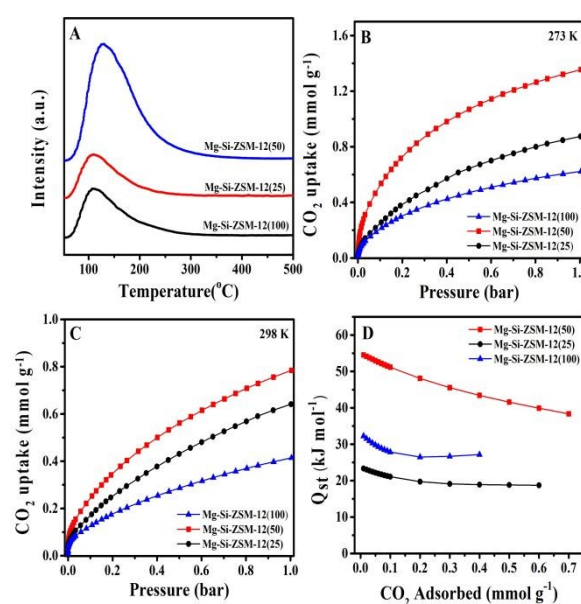
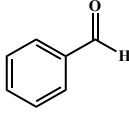
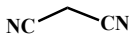
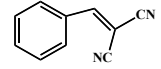
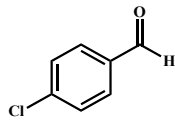
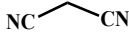
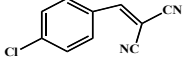
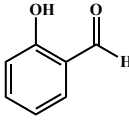
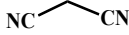
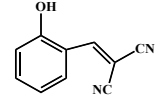
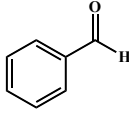
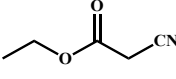
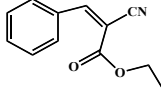
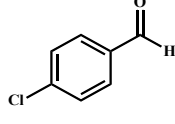
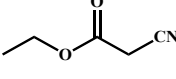
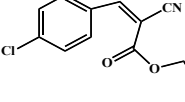
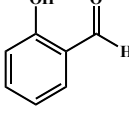
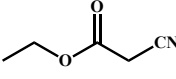
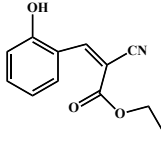
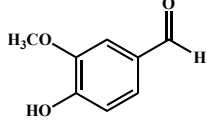
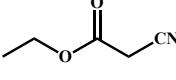
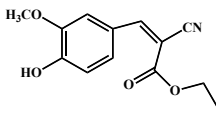


Figure 3 (A) CO<sub>2</sub>-TPD profiles; CO<sub>2</sub> sorption isotherms at (B) 273 K and (C) 298 K; (D) Isothermic heats ( $Q_{\text{st}}$ ) of CO<sub>2</sub> adsorption.

Table 2 Knoevenagel condensation catalyzed by Mg-Si-ZSM-12(50)<sup>a</sup>View Article Online  
DOI: 10.1039/C9CY01329F

Entry	Aromatic aldehyde	Molecule size (Å)	Methylene compounds	Product	Conv. (%) <sup>b</sup>	Blank (%) <sup>c</sup>
1		6.64×4.64			100/37 <sup>d</sup>	27
2		7.25×4.64			100	25
3		6.65×5.41			100	20
4		6.64×4.64			100	20
5		7.25×4.64			100	27
6		6.65×5.41			91	23
7		7.60×6.43			60	20

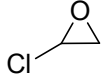
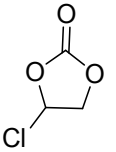
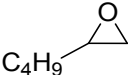
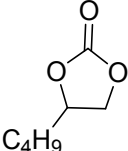
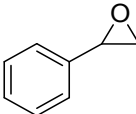
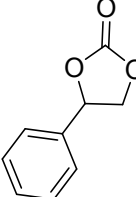
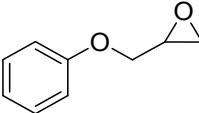
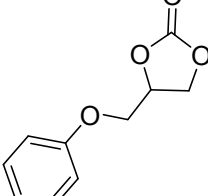
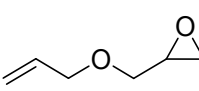
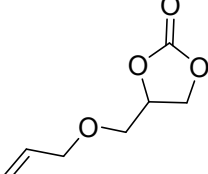
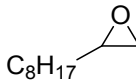
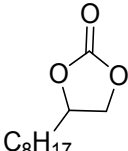
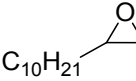
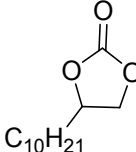
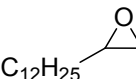
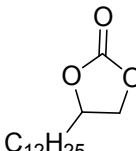
<sup>a</sup>Reaction condition: aromatic aldehydes (8 mmol), ethyl cyanoacetate or malononitrile (8 mmol), catalyst (0.1 g), ethanol (5 mL), 70 °C, 4 h.<sup>b</sup>GC conversion with the selectivity of target product above >99%. <sup>c</sup>Conversion in the absence of catalyst. <sup>d</sup>Knoevenagel condensation between benzaldehyde (5 mmol) and diethyl malonate (5 mmol).m<sup>2</sup> g<sup>-1</sup> and largest pore volume of 0.41 cm<sup>3</sup> g<sup>-1</sup>.

Fig. 1E displays the TG curves of as-synthesized Mg-Si-ZSM-12(*n*) samples. The slow weight loss before 150 °C comes from the water desorption. Drastic weight loss occurs in the temperature range from 150 to 550 °C, attributable to the decomposition of organic template. Only feeble weight loss happened at high temperature above 600 °C, reflecting the well thermal structural stability. Fig. 1F shows the <sup>29</sup>Si MAS NMR spectrum of Mg-Si-ZSM-12(50). Relatively sharp peaks appearing in the range of -105 to -120 ppm are attributable to Q<sup>4</sup> [(Si(OSi)<sub>4</sub>] sites, reflecting the well crystalline structure.<sup>56</sup>

The morphologies of Mg-Si-ZSM-12(*n*) series are reflected by SEM

images in Fig. 2A, 2B and S5†. All of them are the crystallites with well-defined rice-like shape and the size of ca. 1 μm. Amplified SEM image indicated that these particles were aggregations of sheet-like primary particles and closely connected with each other. As the Mg content increases, these particles became flatter and longer, accompanying with increase of their average size. The inset images of Fig. 2B are the corresponding EDX elemental mapping images, depicting a highly dispersive of Mg species. The rice-like morphology was further revealed by TEM image (Fig. 2C). Well-ordered lattice fringe over a large area was observed in the high-resolution TEM image (Fig. 2D), visualizing the crystalline structure.

Table 3 Cycloaddition of CO<sub>2</sub> with epoxides catalyzed by Mg-Si-ZSM-12(50)<sup>a</sup>

Entry	Epoxide	Molecule size (Å)	Product	T [°C]	Time [h]	Conv. [%]	Sel. [%]
1		4.13×3.38		60/150 <sup>b</sup>	10/3 <sup>b</sup>	96/87 <sup>b</sup>	>99/>99 <sup>b</sup>
2		7.21×2.34		90	9	96	96 <sup>c</sup>
3		7.41×4.66		90	9	96	95 <sup>c</sup>
4		8.56×4.67		90	9	95	>99
5		8.62×3.41		90	9	99	95 <sup>c</sup>
6		10.12×3.25		100	9	98	95 <sup>c</sup>
7		12.26×3.32		100	9	98	96 <sup>c</sup>
8		14.31×3.28		100	9	96/28 <sup>d</sup>	96 <sup>c</sup> /99 <sup>d</sup>

<sup>a</sup>Reaction condition: epoxide (5 mmol), catalyst (0.12 g), CO<sub>2</sub> (1.0 bar), TBAB (3 mol%). <sup>b</sup>Activity of Mg-Si-ZSM-12(50) in the absence of TBAB with epichlorohydrin (15 mmol) and CO<sub>2</sub> (3 MPa). <sup>c</sup>Main by-product is 1,2-diol. <sup>d</sup>Activity of TBAB alone (3 mol%).

### Basicity

Incorporation of Mg species into zeolitic skeleton can produce basic sites.<sup>46,57</sup> CO<sub>2</sub>-TPD analysis was utilized to investigate the relative basic strength and total amount of basic sites, according to the peak

position and area. As shown in Fig. 3A, only one desorption peak ranging 50-250 °C appeared in the CO<sub>2</sub>-TPD curves, reflecting that these samples have weak and moderate basicity. The number of basic sites calculated from the desorption peak area is 0.914, 1.451

and 0.892 mmol g<sup>-1</sup> respectively for Mg-Si-ZSM-12(100), Mg-Si-ZSM-12(50) and Mg-Si-ZSM-12(25). Moreover, the desorption peak in the TPD curve of Mg-Si-ZSM-12(50) shifted to higher temperature, reflecting that this sample has superior basicity to the other two.

The static single component CO<sub>2</sub> sorption isotherms of Mg-Si-ZSM-12(*n*) were collected up to 1.0 bar at 273 K and 298 K (Fig. 3B and 3C). At each temperature, the highest CO<sub>2</sub> uptakes of 1.35 mmol g<sup>-1</sup> (273 K, 1 bar) and 0.78 mmol g<sup>-1</sup> (298 K, 1 bar) were achieved on Mg-Si-ZSM-12(50) with the highest Mg content, in line with its superior basicity. The isosteric heat of CO<sub>2</sub> adsorption (*Q<sub>st</sub>*) for Mg-Si-ZSM-12(50), calculated by Virial equation (Fig. S6-S8<sup>†</sup>), gave high value of 54 kJ mol<sup>-1</sup> at zero coverage and decreases slightly along with increasing CO<sub>2</sub> loading (Fig. 3D). The large CO<sub>2</sub> adsorption uptakes and high *Q<sub>st</sub>* of Mg-Si-ZSM-12(50) indicate that this zeolite possesses considerable CO<sub>2</sub> affinity, attributable to the enhanced basicity derived from Mg-incorporation.

### Knoevenagel condensation

Knoevenagel condensation between an active methylene compound and a carbonyl group (C=O) is a classical base-catalyzed reaction for C-C bond coupling to prepare many important chemicals.<sup>58-60</sup> This reaction was preliminarily used to evaluate the base properties of Mg-Si-ZSM-12(50) with the highest Mg content and surface area. Initially, the kinetic curve in the Knoevenagel condensation of benzaldehyde and ethyl cyanoacetate catalyzed by Mg-Si-ZSM-12(50) was compared with that by MgS-1, previous Mg containing zeolite with MFI topology.<sup>39</sup> As shown in Fig. S9<sup>†</sup>, the conversion over Mg-Si-ZSM-12(50) increased with reaction time and reached 100% at 4 h. By contrast, the conversion of blank control was merely 20% in the absence of catalyst (entry 4, Table 2) and 92% by using MgS-1. Besides, the conversion over Mg-Si-ZSM-12(50) was always higher than that over MgS-1 throughout the whole kinetic curves, reflecting the faster reaction rate over Mg-Si-ZSM-12(50). The reason can be assigned to the larger pore of MTW topologic zeolite with the size of (5.6×7.7 Å) than that of MFI type zeolite (5.1×5.5 Å, 5.3×5.6 Å).<sup>61</sup> These results indicate that Mg incorporation into MTW zeolites fabricates active base sites and its 12-membered ring can improve the mass transfer in a heterogeneous catalysis.

The scope of Mg-Si-ZSM-12(50) was investigated in the Knoevenagel condensation of different aromatic aldehydes and ethyl cyanoacetate or malononitrile. Initially, Knoevenagel condensation between benzaldehyde and diethyl malonate was tried, but Mg-Si-ZSM-12(50) exhibited low activity (conversion: 37%, entry 1, Table 2), attributable to the inertness of diethyl malonate.<sup>62</sup> Therefore, Knoevenagel condensation of benzaldehyde and ethyl cyanoacetate or malononitrile were employed to evaluate the activity of Mg-Si-ZSM-12(50). In general, the aromatic aldehydes with electron-donating or electron-withdrawing groups would affect the activity and the later usually affords better performance.<sup>63</sup> Besides, the aromatic aldehydes with different substituted groups significantly influences the mass transfer in the heterogeneous catalysis.<sup>64</sup> Table 2 demonstrates the catalytic results and corresponding molecular sizes of reactants. Nearly complete conversion was observed in the malononitrile related reactions due to the high activity of this substrate. In the Knoevenagel condensation of different aromatic aldehydes and ethyl cyanoacetate, the conversion depends on the molecular size of carbonyl compounds. The conversions were 100%

by using small substrates of benzaldehyde (6.64×4.64 Å) and *p*-chlorobenzaldehyde (7.25×4.64 Å). The larger salicylaldehyde (6.65×5.41 Å) gave a slightly decreased conversion of 91%. The bulky vanillic aldehyde (7.60×6.43 Å) only afforded the conversion of 60%, attributable to the enhanced steric hindrance in the confined space. The diffusion of molecules in the zeolites' microchannels locates in the range of structure-activity diffusion when the size of molecules is close to the pore diameter of zeolites' channels. In such case, the diffusion rate is sensitive to the molecular size. Slightly increasing the molecule size would dramatically enhance the mass transfer resistance. Small size reactant can easily enter the pore channel and access to the active species, facilitating the conversion. The size of bulky vanillic aldehyde (7.60×6.43 Å) is close to that (5.6×7.7 Å) of 12-membered ring of Al-free ZSM-12, and thus its diffusion in the microchannels is limited, demonstrating the low activity. In the Knoevenagel condensation, the size of carbonyl compounds is larger than ethyl cyanoacetate or malononitrile, therefore the conversion depends on the molecular size of the carbonyl compounds. Compared with previous heteroatom zeolites and zeolitic-like materials in this reaction,<sup>47,65, 66</sup> Mg-Si-ZSM-12(50) exhibits superior activity in converting a broad spectrum of substrates.

### Cycloaddition of CO<sub>2</sub> with epoxides

Given the superior basic properties, Mg-Si-ZSM-12(50) was further used as a heterogeneous catalyst in the solvent-free cycloaddition of CO<sub>2</sub> with epoxides to produce cyclic carbonates (Table 3). Mg-Si-ZSM-12(50) exhibited high activity and selectivity towards a variety of terminal epoxides under mild conditions of atmospheric CO<sub>2</sub> pressure and relatively low temperature (≤100 °C) in the presence of a conventional additive of tetrabutylammonium bromide (TBAB). The pore size of the orifice (5.6×7.7 Å) is larger than the epoxides in Table 3, and thus these substrates can enter the microchannels of Mg-Si-ZSM-12 and then converted into corresponding cyclic carbonates. In addition, the adsorption kinetic curve of 1,2-epoxytetradecane (the most bulky epoxide in this work) on Mg-Si-ZSM-12(50) was collected and compared with that on Mg-Si-ZSM-12(50)-as (the as-synthesized Mg-Si-ZSM-12(50) without the removal of template, a nonporous counterpart of Mg-Si-ZSM-12(50)). As displayed in Fig. S10<sup>†</sup>, continuous adsorption of 1,2-epoxytetradecane on Mg-Si-ZSM-12(50) was observable, whereas rare adsorption occurred on Mg-Si-ZSM-12(50)-as due to the blockage of pore by the organic template. This phenomenon validates the entrance of the bulky epoxide into the internal micropores of Mg-Si-ZSM-12(50). This is in line with previous catalytic behavior of zeolites and related microporous materials in isomerization of long-chain *n*-alkanes (>C<sub>10</sub>),<sup>67,68</sup> and the results of cycloaddition of CO<sub>2</sub> with bulky epoxides catalyzed by Metal-Organic Frameworks (MOFs) with micropores.<sup>69,70</sup> Terminal epoxide with electron-withdrawing group (epichlorohydrin) was transformed completely (conversion: 96%, selectivity: >99%) at a low temperature of 60 °C (entry 1). Mg-Si-ZSM-12(50) catalyzed cycloaddition of CO<sub>2</sub> with epichlorohydrin was carried out at different temperatures and the kinetic curves at 60 and 80 °C were collected (Fig. S11<sup>†</sup>). With the elevated temperature, the conversion increased from 70% (40 °C) to 99% (70 and 80 °C) (Fig. S11A<sup>†</sup>). In addition, rapid conversion rate was observed at 80 °C than that at 60 °C (Fig. S11B<sup>†</sup>). Slightly increasing the temperature to be 90 °C enabled the high activity in

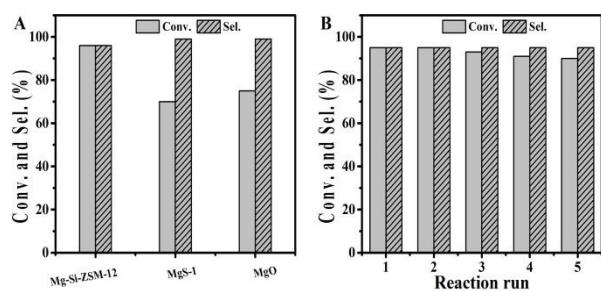


Figure 4 (A) Cycloaddition of CO<sub>2</sub> with 1,2-epoxyhexane. Reaction condition: 1,2-epoxyhexane (5 mmol), catalyst (0.12 g), CO<sub>2</sub> (1.0 bar), TBAB (3 mol%, 0.048 g), 90 °C, 9 h; (B) Reusability of Mg-Si-ZSM-12(50) in the cycloaddition of CO<sub>2</sub> with styrene oxide. Reaction condition: styrene oxide (5 mmol), catalyst (0.12 g), CO<sub>2</sub> (1.0 bar), TBAB (3 mol%, 0.048 g), 90 °C, 9 h.

the coupling of CO<sub>2</sub> with terminal epoxides containing either short-chain branch or benzene ring (entry 2-5). Even the inert long carbon-chain alkyl epoxides were effectively coupled with atmospheric CO<sub>2</sub> into the corresponding cyclic carbonates with high conversions and selectivities at 100 °C (entry 6-8). Herein, to the best of our knowledge, it is the first time to reach the efficient conversion of a broad spectrum of epoxides into cyclic carbonates over zeolite catalysts. The activity of Mg-Si-ZSM-12(50) outperforms previous zeolites that usually catalyzed the cycloaddition of CO<sub>2</sub> with epoxides under high pressure and temperature.<sup>22,23</sup> Mg-Si-ZSM-12(50) also exhibited superior or at least comparable yield to previous zeolite analogues such as multifunctional lanthanide-zeolites in the conversion of epichlorohydrin, styrene oxide and so on.<sup>24</sup> More importantly, it was found that Mg-Si-ZSM-12(50) effectively transformed various inert long alkyl chain epoxides in the presence of atmospheric CO<sub>2</sub>, which was normally catalyzed by those most efficient ionic liquids derived materials.<sup>71-73</sup> All of these reveal the high efficiency of constructed Mg-containing MTW zeolite in this CO<sub>2</sub> fixation under mild conditions.

For comparison, the activity of Mg-Si-ZSM-12(50) was compared with MgS-1 and commercial solid base MgO in the CO<sub>2</sub> cycloaddition with 1,2-epoxyhexane (Fig. 4A). The conversion was only 70% by using MgS-1 and even lower than that (75%) in the MgO catalyzed reaction. By contrast, Mg-Si-ZSM-12(50) demonstrated a greatly enhanced yield of 96% under the identical reaction condition. The higher activity of Mg-Si-ZSM-12(50) relative to those of MgO and MgS-1 highlights the significance of generating superior basic sites in the zeolites' skeleton. On the contrary, the conversion was 49% when the reaction was catalyzed by 3 mol% of TBAB alone, and increased to be 60%, 71% and 83% by using 6 mol%, 9 mol%, and 12 mol% of TBAB (Fig. S12<sup>†</sup>). TBAB was widely used as the efficient co-catalyst in the CO<sub>2</sub> cycloaddition with epoxides.<sup>74-77</sup> For example, FJI-H14 catalyzed cycloaddition of CO<sub>2</sub> with styrene oxide resulted in a yield of 86% in the presence of TBAB, while TBAB (2.5 mol%) alone gave a yield of 52% under the identical conditions.<sup>74</sup> The yield was 99% when CO<sub>2</sub> cycloaddition with epichlorohydrin catalyzed by Cu/POP-Bpy and TBAB, while changed to be 60.2% by using TBAB (7 mol%).<sup>75</sup> Besides, slightly lower yields were observable in many other cycloadditions catalyzed by TBAB.<sup>76,77</sup> These phenomena suggest

that the activity of TBAB alone varied with the reaction conditions. In order to unravel the catalytic behavior of TBAB, TBAB catalyzed conversion of 1,2-epoxytetradecane via cycloaddition with CO<sub>2</sub> was carried under the chosen reaction condition (entry 8, Table 3). The conversion was 28% by using TBAB alone, whereas increased to be 96% when the reaction was catalyzed by Mg-Si-ZSM-12(50) and TBAB (entry 8, Table 3). This result further reveals the synergistic catalysis of Mg-Si-ZSM-12(50) and TBAB.

In situ FT-IR spectra of adsorbed CO<sub>2</sub> and epoxide (epoxypropane) on Mg-Si-ZSM-12(50) were collected respectively to gain insight into Mg-Si-ZSM-12(50) catalyzed CO<sub>2</sub> cycloaddition with epoxide. Fig. S13A<sup>†</sup> shows the IR spectra of adsorbed CO<sub>2</sub> on Mg-Si-ZSM-12(50) under dynamic CO<sub>2</sub> atmosphere. The peaks around 1680 and 1600 cm<sup>-1</sup> are attributable to the asymmetric and symmetric stretching vibrations of carbonyl group and these characteristic peaks of C=O increased with the adsorption duration, suggesting the formation of carbonate.<sup>78,79</sup> The IR spectra of epoxypropane adsorbed on Mg-Si-ZSM-12(50) were shown in Fig. S13B<sup>†</sup>. The peaks around 2996 cm<sup>-1</sup> are assignable to the stretching vibration of C-H bond; further peaks at 1470 and 1400 cm<sup>-1</sup> are attributed to the C-H bending vibration of three-membered epoxy ring and CH<sub>3</sub> connected to the epoxy ring, respectively. The epoxide ring breathing and stretching vibration of C-O were reflected by the peaks of 1265 and 1120 cm<sup>-1</sup>. The emerging of these peaks with certain shifts from those observed in liquid epoxypropane,<sup>80,81</sup> suggests the chemisorption of epoxide on Mg-Si-ZSM-12(50). This is further reflected by the observation of the negative peak at 3700 cm<sup>-1</sup>, which is attributable to the interaction of surface hydroxyl groups and epoxypropane. Generally, three primary steps of ring-opening via nucleophilic attack, CO<sub>2</sub> insertion, and ring-closure with the leaving of nucleophile are involved in the CO<sub>2</sub> cycloaddition with epoxides. The ring opening step can be facilitated by the activation of epoxides by a H-bonding donor or Lewis acid compound and then attached by nucleophiles such as halide ions.<sup>82,83</sup> Based on these studies and the in situ FT-IR result, the probable reaction routes in the absence and presence of TBAB are proposed in Scheme S1<sup>†</sup>(ESI). Epoxide is adsorbed and activated on the Mg sites through the static electron interaction between the O atom of epoxide and Mg cations. Besides, the surface hydroxyl groups also served as hydrogen bond donors to activate epoxides.<sup>84,85</sup> CO<sub>2</sub> was adsorbed on the surface to form carbonate species via interacting with the basic sites (e.g., the oxygen linked with Mg (O-Mg)). In the absence of TBAB, these carbonates served as the nucleophile to attack the less steric hindered carbon atom of the epoxide to generate the intermediate by inserting CO<sub>2</sub> into the covalent bond of C-O (Scheme S1A<sup>†</sup>).<sup>15,22,86</sup> Therefore, Mg-Si-ZSM-12(50) alone also can catalyze the CO<sub>2</sub> cycloaddition with epoxide under high temperature and pressure. For instance, Mg-Si-ZSM-12(50) itself gave a conversion of 87% (selectivity: >99%) in catalyzing the CO<sub>2</sub> cycloaddition with epichlorohydrin (entry 1, Table 3). In the presence of TBAB, the more nucleophilic reagent, Br<sup>-</sup> from TBAB can accelerate the ring-opening to yield Br-substituted intermediate, which further interact with the adsorbed CO<sub>2</sub> to cause the CO<sub>2</sub> insertion (Scheme S1B<sup>†</sup>). The final product cyclic carbonate is obtained with the ring closure of the intermediates above. The potential bi-product 1,2-diol formed via the ring-opening of epoxide by trace water (Scheme S1C<sup>†</sup>).<sup>87,88</sup> The high performance comes from a synergistic effect of Mg-Si-ZSM-12(50) and TBAB. Especially, the

superior basicity of Mg-Si-ZSM-12(50) is beneficial for CO<sub>2</sub> activation. Though the epoxide activation is crucial as the first step is normally the rate-determining step, CO<sub>2</sub> activation also significantly contributes the catalytic performance. The combination of CO<sub>2</sub>-TPD analysis, static CO<sub>2</sub> adsorption and activity evaluation Knoevenagel condensation, indicated that Mg-Si-ZSM-12(50) has superior basicity. In addition, Mg-Si-ZSM-12(50) exhibited higher conversion over Mg-Si-ZSM-12(50) than MgO and MgS-1 in the CO<sub>2</sub> cycloaddition with epoxide. These phenomena suggest that the superior basicity of Mg-Si-ZSM-12(50) is important for the CO<sub>2</sub> activation and corresponding to its higher activity in the CO<sub>2</sub> cycloaddition with epoxide. The potential advantage of Mg-Si-ZSM-12(50) also include abundant micropores and mesopores that promote the dispersion and accessibility of the basic sites. Compared with previous MgS-1 with relatively small 10-membered ring, Mg-Si-ZSM-12(50) possessing larger 12-membered ring channels provides improved mass transfer and thus promotes the activity, in line with the results found in the Knoevenagel condensation. To evaluate the catalyst's reusability, a five-run recycling test was carried out in the coupling of atmospheric CO<sub>2</sub> with styrene oxide. As shown in Fig. 4B, the conversion and selectivity of the product obtained from the second to fifth runs were similar to that of the fresh catalyst, reflecting the favorable recycling performance.

## Conclusions

In summary, a family of zeolitic solid base with well-defined 12-MR channels (Mg-Si-ZSM-12) was fabricated by incorporating Mg species into MTW type zeolite. The synthesis was achieved in an acid co-hydrolysis route. The obtained zeolite exhibited improved basic properties, and hence served as efficient solid base in traditional base reaction (Knoevenagel condensation) and cycloaddition of CO<sub>2</sub> with epoxides under relative mild conditions. This work highlights the potential of basic zeolites in the CO<sub>2</sub> fixation.

## Conflicts of interest

There are no conflicts to declare.

## Acknowledgements

The authors thank the National Natural Science Foundation of China (No. U1662107, 21476109, 21136005 and 21303084) and the Project of Priority Academic Program Development of Jiangsu Higher Education Institutions (PAPD).

## Notes and references

- 1 A. Banerjee, G. R. Dick, T. Yoshino and M. W. Kanan, *Nature*, 2016, **531**, 215.
- 2 J. Klankermayer, S. Wesselbaum, K. Beydoun and W. Leitner, *Angew. Chem. Int. Ed.*, 2016, **55**, 7296.
- 3 M. Alves, B. Grignard, R. Mereau, C. Jerome, T. Tassaing and C. Detrembleur, *Catal. Sci. Technol.*, 2017, **7**, 2651.
- 4 L. Zhang, Z. J. Zhao and J. L. Gong, *Angew. Chem. Int. Ed.*, 2017, **56**, 11326. View Article Online  
DOI: 10.1039/C9CY01329F
- 5 F. J. Quan, G. M. Zhan, C. L. Mao, Z. H. Ai, F. L. Jia, L. Z. Zhang, H. G. Gu and S. Y. Liu, *Catal. Sci. Technol.*, 2018, **8**, 6503.
- 6 M. W. Jia, C. Choi, T. S. Wu, C. Ma, P. Kang, H. C. Tao, Q. Fan, S. Hong, S. Z. Liu, Y. Soo, Y. Jung, J. S. Qiu and Z. Y. Sun, *Chem. Sci.*, 2018, **9**, 8775.
- 7 A. Bansode and A. Urakawa, *ACS Catal.*, 2014, **4**, 3877.
- 8 H. Zhong, G. D. Yao, X. Cui, P. Yan, X. G. Wang and F. M. Jin, *Chem. Eng. J.*, 2019, **357**, 421.
- 9 W. F. Xiong, C. R. Qi, H. T. He, L. Ouyang, M. Zhang and H. F. Jiang, *Angew. Chem. Int. Ed.*, 2015, **54**, 3084.
- 10 Q. W. Song, Z. H. Zhou and L. N. He, *Green Chem.*, 2017, **19**, 3707.
- 11 C. Maeda, S. Sasaki and T. Ema, *ChemCatChem*, 2017, **9**, 946.
- 12 J. Liang, R. P. Chen, X. Y. Wang, T. T. Liu, X. S. Wang, Y. B. Huang and R. Cao, *Chem. Sci.*, 2017, **8**, 1570.
- 13 J. F. Kurisingal, R. Babu, S. H. Kim, Y. X. Li, J. S. Chang, S. J. Cho and D. W. Park, *Catal. Sci. Technol.*, 2018, **8**, 591.
- 14 K. Yamaguchi, K. Ebitani, T. Yoshida and K. Kaneda, *J. Am. Chem. Soc.*, 1999, **121**, 4526.
- 15 Z. J. Guo, X. C. Cai, J. Y. Xie, X. C. Wang, Y. Zhou and J. Wang, *ACS Appl. Mater. Interfaces*, 2016, **8**, 12812.
- 16 P. Z. Li, X. J. Wang, J. Liu, J. S. Lim, R. Zou and Y. Zhao, *J. Am. Chem. Soc.*, 2016, **138**, 2142.
- 17 B. Dong, L. Y. Wang, S. Zhao, R. Ge, X. D. Song, Y. Wang and Y. N. Gao, *Chem. Commun.*, 2016, **52**, 7082.
- 18 W. L. Wang, C. Y. Li, L. Yan, Y. Q. Wang, M. Jiang and Y. J. Ding, *ACS Catal.*, 2016, **6**, 6091.
- 19 J. Zhang, L. Wang, Y. Shao, Y. Q. Wang, B. C. Gates and F. S. Xiao, *Angew. Chem. Int. Ed.*, 2017, **56**, 9747.
- 20 G. Q. Zhang, P. Feng, W. P. Zhang, H. Liu, C. X. Wang, H. J. Ma, D. D. E. Wang and Z. J. Tian, *Microporous Mesoporous Mater.*, 2017, **247**, 158.
- 21 V. J. Margarit, M. E. Martnez-Armero, M. T. Navarro, C. Martnez and A. Corma, *Angew. Chem. Int. Ed.*, 2015, **54**, 13724.
- 22 M. Tu and R. J. Davi, *J. Catal.*, 2001, **199**, 85.
- 23 C. G. Li, L. Xu, P. Wu, H. H. Wu and M. Y. He, *Chem. Commun.*, 2014, **50**, 15764.
- 24 J. Dong, P. Cui, P. F. Shi, P. Cheng and B. Zhao, *J. Am. Chem. Soc.*, 2015, **137**, 15988.
- 25 H. Li, Z. Fang, J. Luo and S. Yang, *Appl. Catal. B: Environ.*, 2017, **200**, 182.
- 26 R. Locus, D. Verboekend, R. Zhong, K. Houthoofd, T. Jaumann, S. Oswald, L. Giebel, G. Baron and B. F. Sels, *Chem. Mater.*, 2016, **28**, 7731.
- 27 L. Zhang, T. N. Pham, J. Faria, D. Santhanaraj, T. Sooknoi, Q. H. Tan, Z. Zhao and D. E. Resasco, *ChemSusChem*, 2016, **7**, 736.
- 28 S. C. Chen, Z. Shao, Z. X. Fang, Q. Chen, T. Tang, W. Q. Fu, L. Zhang and T. D. Tang, *J. Catal.*, 2016, **338**, 38.
- 29 M. Miyamoto, T. Nakatani, Y. Fujioka and K. Yogo, *Microporous Mesoporous Mater.*, 2015, **206**, 67.
- 30 A. Corma, F. Rey, J. Rius, M. J. Sabater and S. Valencia, *Nature*, 2004, **431**, 287.
- 31 B. W. Boal, J. E. Schmidt, M. A. Deimund, M. W. Deem, L. M. Henling, S. K. Brand, S. I. Zones and M. E. Davis, *Chem. Mater.*, 2015, **27**, 7774.
- 32 C. W. Lopes, L. G. Hortigüela, A. Rojas and S. B. C. Pergher, *Microporous Mesoporous Mater.*, 2017, **252**, 29.
- 33 Y. X. Li, D. Bernin, F. F. Gao and N. Hedin, *Microporous Mesoporous Mater.*, 2017, **237**, 222.
- 34 H. M. Wen, Y. Zhou, J. Y. Xie, Z. Y. Long, W. Zhang and J. Wang, *RSC Adv.*, 2014, **4**, 49647.
- 35 S. Song, G. J. Wu, W. L. Dai, N. J. Guan and L. D. Li, *Catal. Sci. Technol.*, 2016, **6**, 8325.
- 36 H. Xu, X. D. Wang, P. Ji, H. H. Wu, Y. J. Guan and P. Wu, *Inorg. Chem. Front.*, 2018, **5**, 2763.

- 37 Z. Sun, T. Li, G. Li, Y. H. Zhang and Y. Tang, *RSC Adv.*, 2017, **7**, 35252.
- 38 A Thangaraj, M. J. Eapen, S. Sivasanker and P. Ratnasamy, *Zeolites*, 1992, **12**, 943.
- 39 Y. Zhou, Y. H. Jin, M. Wang, W. Zhang, J. Y. Xie, J. Gu, H. M. Wen, J. Wang and L. M. Peng, *Chem. Eur. J.*, 2015, **21**, 15412.
- 40 Y. J. Wu, J. Wang, P. Liu, W. Zhang, J. Gu and X. J. Wang, *J. Am. Chem. Soc.*, 2010, **132**, 17989.
- 41 W. Zhang, W. Hou, T. S. Meng, W. X. Zhuang, J. Y. Xie, Y. Zhou and J. Wang, *Catal. Sci. Technol.*, 2017, **7**, 6050.
- 42 J. Gu, Y. H. Jin, Y. Zhou, M. J. Zhang, Y. J. Wu and J. Wang, *J. Mater. Chem. A*, 2013, **1**, 2453.
- 43 J. Y. Xie, W. X. Zhuang, N. Yan, Y. H. Du, S. B. Xi, W. Zhang, J. J. Tang, Y. Zhou and J. Wang, *Chem. Eng. J.*, 2017, **328**, 1031.
- 44 Q. G. Zhai, X. H. Bu, C. Y. Mao, X. Zhao and P. Y. Feng, *J. Am. Chem. Soc.*, 2016, **138**, 2524.
- 45 D. F. Shantz, H. Koller and R. F. Lobo, *J. Am. Chem. Soc.*, 2000, **122**, 6659.
- 46 J. Y. Xie, W. X. Zhuang, W. Zhang, Y. Zhou and J. Wang, *ChemCatChem*, 2017, **9**, 1076.
- 47 G. D. Feng, P. Cheng, W. F. Yan, M. Boronat, X. Li, J. H. Su, J. Y. Wang, Y. Li, A. Corma, R. R. Xu and J. H. Yu, *Science*, 2016, **351**, 1188.
- 48 Y. X. Tan, F. Wang and J. Zhang, *Chem. Soc. Rev.*, 2018, **47**, 2130.
- 49 W. Zhang, J. Y. Xie, W. Hou, Y. Q. Liu, Y. Zhou and J. Wang, *ACS Appl. Mater. Interfaces*, 2016, **8**, 23122.
- 50 Y. Li, Z. C. Feng, Y. X. Lian, K. Q. Sun, L. Zhang, G. Q. Jia, Q. H. Yang and C. Li, *Microporous Mesoporous Mater.*, 2005, **84**, 41.
- 51 C. Paris, N. Martin, J. Martinez-Triguero, M. Moliner and A. Corma, *New J. Chem.*, 2016, **40**, 4140.
- 52 J. Y. Xie, H. M. Wen, W. Zhang, Y. Zhou and J. Wang, *CrystEngComm*, 2016, **18**, 1164.
- 53 M. M. Forde, R. D. Armstrong, C. J. Kiely and G. J. Hutchings, *J. Am. Chem. Soc.*, 2013, **135**, 11087.
- 54 K. S. W. Sing, D. H. Everett, R. A. W. Haul, L. Moscou, R. A. Pierotti, J. Rouquerol and T. Siemieniewska, *Pure Appl. Chem.*, 1985, **57**, 603.
- 55 Y. Kamimura, K. Iyoki, S. P. Elangovan, K. Itabashi, A. Shimojima and T. Okubo, *Microporous Mesoporous Mater.*, 2012, **163**, 282.
- 56 K. Arishtirova, P. Kovacheva and N. Davidova, *Appl. Catal. A-Gen.*, 1998, **167**, 271.
- 57 F. Frusteri, M. Cordaro, C. Cannilla and G. Bonura, *Appl. Catal. B: Environ.*, 2015, **162**, 57.
- 58 L. Zhu, X. Q. Liu, H. L. Jiang and L. B. Sun, *Chem. Rev.*, 2017, **117**, 8129.
- 59 Y. Zhang, Y. X. Wang, L. Liu, N. Wei, M. L. Gao, D. Zhao and Z. B. Han, *Inorg. Chem.*, 2018, **57**, 2193.
- 60 H. F. Wang, C. Y. Wang, Y. F. Yang, M. Zhao and Y. J. Wang, *Catal. Sci. Technol.*, 2017, **7**, 405.
- 61 C. A. Fyfe, H. Gies, G. T. Kokotailo, B. Marler and D. E. Cox, *J. Phys. Chem.*, 1990, **94**, 3718.
- 62 K. Sugahara, T. Kimura, K. Kamata, K. Yamaguchi and N. Mizuno, *Chem. Commun.*, 2012, **48**, 8422.
- 63 Y. Ogiwara, K. Takahashi, T. Kitazawa and N. Sakai, *J. Org. Chem.*, 2015, **80**, 3101.
- 64 H. Zhu, L. F. Xiong, M. H. Zhou and K. Huang, *Polym. Chem.*, 2016, **7**, 4975.
- 65 H. K. Min, S. H. Cha and S. B. Hong, *Chem. Commun.*, 2013, **49**, 1115.
- 66 V. N. Panchenko, M. M. Matrosova, J. Jeon and S. H. Jung, *J. Catal.*, 2014, **316**, 251.
- 67 C. Zschiesche, D. Himsel, R. Rakoczy, A. Reitzmann, J. Freiding, N. Wilde and R. Gläser, *Chem. Eng. Technol.*, 2018, **41**, 199.
- 68 M. Zhang, Y. J. Chen, L. Wang, Q. M. Zhang, C. Tsang and C. H. Liang, *Ind. Eng. Chem. Res.*, 2016, **55**, 6069.
- 69 W. Jiang, J. Yang, Y. Y. Liu, S. Y. Song and J. F. Ma, *Chem. Eur. J.*, 2016, **22**, 16991. View Article Online  
DOI: 10.1039/C9CY01329F
- 70 J. Liang, R. P. Chen, X. Y. Wang, T. T. Liu, X. S. Wang, Y. B. Huang and R. Cao, *Chem. Sci.*, 2017, **8**, 1570.
- 71 S. Ghazali-Esfahani, H. B. Song, E. Păunescu, F. D. Bobbink, H. Z. Liu, Z. F. Fei, G. Laurenczy, M. Bagherzadeh, N. Yan and P. J. Dyson, *Green Chem.*, 2013, **15**, 1584.
- 72 W. Zhang, T. Y. Liu, H. H. Wu, P. Wu and M. Y. He, *Chem. Commun.*, 2015, **51**, 682.
- 73 R. R. Shaikh, S. Pornpraprom and V. D'Elia, *ACS Catal.*, 2018, **8**, 419.
- 74 L. F. Liang, C. P. Liu, F. L. Jiang, Q. H. Chen, L. J. Zhang, H. Xue, H. L. Jiang, J. J. Qian, D. Q. Yuan and M. C. Hong, *Nat. Commun.*, 2017, **8**, 1233.
- 75 Z. F. Dai, Q. Sun, X. L. Liu, L. P. Guo, J. X. Li, S. X. Pan, C. Q. Bian, L. Wang, X. Hu, X. J. Meng, L. H. Zhao, F. Deng and F. S. Xiao, *ChemSusChem*, 2017, **10**, 1186.
- 76 Z. F. Dai, Q. Sun, X. L. Liu, C. Q. Bian, Q. M. Wu, S. X. Pan, L. Wang, X. J. Meng, F. Deng and F. S. Xiao, *J. Catal.*, 2016, **338**, 202.
- 77 Y. Xie, T. T. Wang, X. H. Liu, K. Zou and W. Q. Deng, *Nat. Commun.*, 2013, **4**, 1960.
- 78 C. Knöfel, C. Martin, V. Hornebecq and P. L. Liewellyn, *J. Phys. Chem. C*, 2009, **113**, 21726.
- 79 Y. Zhou, W. L. Zhang, L. Ma, Y. Zhou and J. Wang, *ACS Sustainable Chem. Eng.*, 2019, **7**, 9387.
- 80 G. Mul, A. Zwijnenburg, B. V. D. Linden, M. Makkee and J. A. Moulijn, *J. Catal.*, 2001, **201**, 128.
- 81 W. Zhang, H. Wang, Q. Li, Q. Dong, N. Zhao, W. Wei, Y. Sun, *Appl. Catal. A: Gen.* 2005, **294**, 188.
- 82 F. D. Bobbink and P. J. Dyson, *J. Catal.*, 2016, **343**, 52.
- 83 F. D. Bobbink, D. Vasilyev, M. Hulla, S. Chamam, F. Menoud, G. Laurenczy, S. Katsyuba and P. J. Dyson, *ACS Catal.*, 2018, **8**, 2589.
- 84 C. L. Thomas, *Ind. Eng. Chem.*, 1949, **41**, 2564.
- 85 L. Sandoval-Díaz, J. González-Amaya and C. Trujillo, *Microporous Mesoporous Mater.*, 2015, **215**, 229.
- 86 T. Ema, K. Fukuhara, T. Sakai, M. Ohbo, F. Q. Bai and J. Y. Hasegawa, *Catal. Sci. Technol.*, 2015, **5**, 2314.
- 87 Y. Morimoto, E. Takeuchi, H. Kambara, T. Kodama, Y. Tachi and K. Nishikawa, *Org. Lett.*, 2013, **15**, 2966.
- 88 J. Liang, L. N. Soucie, D. R. Blechschmidt, A. Yoder, A. Gustafson and Y. Liu, *Org. Lett.*, 2019, **21**, 513.

# Straightforward synthesis of MTW-type magnesium silicalite for CO<sub>2</sub> fixation with epoxides under mild conditions†

Haimeng Wen,<sup>a</sup> Jingyan Xie,<sup>a,b</sup> Yang Zhou,<sup>a</sup> Yu Zhou<sup>\*a</sup> and Jun Wang<sup>\*a</sup>

<sup>a</sup>State Key Laboratory of Materials-Oriented Chemical Engineering, College of Chemical Engineering, Nanjing Tech University, Nanjing 210009, Jiangsu, P. R. China.

<sup>b</sup>Maoming Branch R&D Institute, SINOPEC, Maoming 525011, P. R. China.

† These two authors contributed equally: Haimeng Wen and Jingyan Xie.

\* Corresponding authors

E-mails: njtzhouyu@njtech.edu.cn (Y. Zhou), junwang@njtech.edu.cn (J. Wang)



Mg-Si-ZSM-12 was hydrothermally synthesized and effective for CO<sub>2</sub> fixation under mild conditions.